

# Fiber Engineering Trifecta of Spinnability, Morphology, and Properties: Centrifugally Spun versus Electrospun Fibers

Jorgo Merchiers,<sup>||</sup> Cheryl Lynn Slykas,<sup>||</sup> Carina D. V. Martínez Narváez, Mieke Buntinx, Wim Deferme, Roos Peeters, Naveen K. Reddy,<sup>\*</sup> and Vivek Sharma<sup>\*</sup>



Cite This: <https://doi.org/10.1021/acscapm.1c01865>



Read Online

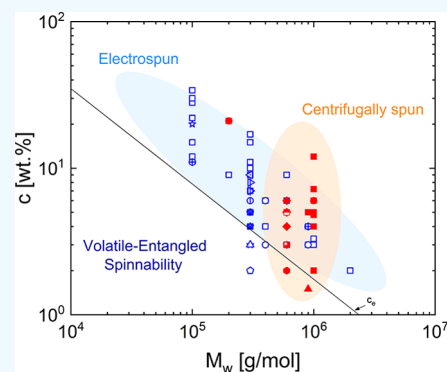
ACCESS |

Metrics & More

Article Recommendations

**ABSTRACT:** Designing application-ready fibers involves multifaceted challenges related to correlating the formulation properties and processing parameters to the fiber engineering trifecta of spinnability, morphology, and properties. Here, we characterize the influence of macromolecular and solvent properties on the trifecta for poly(ethylene oxide) (PEO) fibers produced using a bespoke centrifugal force spinning (CFS) setup and matched processing parameters. We illustrate the influence of changing solvent on spinnability, morphology, and properties (thermal and mechanical) by varying the acetonitrile (AcN) fraction in the spinning dope formulated with PEO dissolved in AcN/H<sub>2</sub>O mixtures. We contrast the numerical values of measured diameter, tensile strength, elongation-at-break, and crystallinity of centrifugally spun PEO fibers with the published data sets for electrospun fibers using the Berry number (or the overlap parameter) as the ordinate. We compile, analyze, and replot ES and CFS data sets obtained for various solvents, PEO ( $M_w$  and  $c$ ), and processing parameters. Even though distinct forces determine the jet trajectory and fiber formation for ES and CFS, we find that centrifugally spun PEO fibers emulate electrospun fiber properties, morphology, and spinnability. We discuss the mechanism underlying volatile-entangled spinnability, displayed here by PEO solutions in certain AcN/H<sub>2</sub>O mixtures, in contrast to extensibility-enriched spinnability of multicomponent formulations, enabled by the addition of an ultrahigh  $M_w$  polymer fraction.

**KEYWORDS:** centrifugal spinning, spinnability, rheology, entangled polymers, electrospinning, rotary jet spinning, nonwovens



## INTRODUCTION

An astute selection of material and processing parameters to facilitate the production of fibers with desirable diameter, morphology, crystallinity, and mechanical properties presents a set of grand challenges for applied polymer and fiber science.<sup>1–7</sup> Despite the availability of high quality, produced on large commercial-scale fibers including rayon, nylon, poly(ethylene terephthalate), polypropylene, poly(acrylonitrile), and Kevlar, to name a few, considerable demand exists for bench-scale methods to produce fibers for specialized end-user applications, optimizing ingredients, and meeting multiple functionality targets. For example, high surface area, mesh-like nonwoven structures produced on-demand are sought for biomedical applications such as wound dressing, drug delivery, and tissue engineering.<sup>8–10</sup> Control over the surface area and porosity are desirable for applications in water purification, separation and filtration,<sup>11–13</sup> and energy storage and production.<sup>14–16</sup> Many applications require composite fibers with additives such as nanoparticles to control conductivity, modulus, catalytic or antibacterial properties. Composite fibers are often loaded with proteins and even cells for biomedical applications, APIs (active pharma ingredients) for drug delivery, and fungi, pesticides, or

fertilizers in agriculture applications.<sup>10,17–22</sup> Emerging applications in the food sector include creating fibrous structures for improving texture, packaging fruits, or protecting seeds with gossamer thin coatings.<sup>21</sup> The production of fibers with desired properties, cost, quantities, and application-suited functionalities requires the exposition and investigation of the fiber engineering trifecta: (i) spinnability, (ii) morphology, and (iii) fiber properties. In this contribution, we investigate the trifecta for centrifugally spun poly(ethylene oxide) (PEO) fibers and highlight the similarities and the contrast with electrospun PEO fibers. The choice of PEO as the model system presents an opportunity to benefit from the extensive fundamental studies of its crystallization behavior,<sup>23,24</sup> rheological response<sup>25–28</sup> (including by the coauthors<sup>29–33</sup>), and fiber formation using

**Received:** December 21, 2021

**Accepted:** January 31, 2022

electrospinning (ES) and centrifugal force spinning (CFS), as discussed herein.

Despite the relative success of ES for producing submicron and nanoscopic fibers using various polymers, the need for high voltage sources, low production rates, and limited range of spinnable formulations has driven the search for alternatives<sup>4–7,10,34,35</sup> including CFS,<sup>6,35–37</sup> melt-blown,<sup>38,39</sup> template synthesis,<sup>40</sup> phase separation,<sup>41</sup> and CO<sub>2</sub> laser supersonic drawing,<sup>42</sup> among others. However, designing application-ready fibers involves multifaceted challenges<sup>1–6,21,28,34–56</sup> related to correlating the processing parameters and formulation properties, including rheological response to the trinity of spinnability, morphology, and properties that we refer to as the fiber engineering trifecta. CFS features a spiraling jet ejected from a fast-rotating spinneret or nozzles under the influence of centrifugal forces. Contrastingly, in ES, electrostatic forces draw a pendant droplet of a viscoelastic, polymeric liquid into a Taylor cone that first creates a charged fluid jet that travels in a gyrating trajectory toward the grounded collector.<sup>3,4,35,57,58</sup> Even though cotton candy and glass wool, centrifugally spun from viscous melts, have existed for over a century, research on fibers centrifugally spun from viscoelastic polymer solutions took off just over a decade back, under many avatars: CFS, centrifugal spinning, force spinning, rotary spinning, rotary jet spinning, or cotton candy process.<sup>6,7,35–37,43,45,59–64</sup> Thus, challenges specific to viscoelastic free surface flows and instabilities influence the formation of centrifugally spun polymeric fibers. Despite the difference in driving electrostatics versus centrifugal forces, jets formed in both ES and CFS undergo drawing and thinning, and bending instabilities, subject to an influence of stresses due to viscoelasticity, viscosity, capillarity, air drag, inertia, and gravity.<sup>44,45,65,66</sup> In both ES and CFS, evaporative loss of solvent, leading to the formation of solidified fiber mats occurs for suitable nozzle–collector distances. Several questions underlying the fiber engineering trifecta that remain unaddressed for CFS motivate this study. We contextualize and contrast the CFS observations and findings with ES studies and contend that addressing these challenges is necessary for taking the advantage of higher production rates (compared to ES) and producing fibers from a wide variety of polymer solutions or melts and multicomponent formulations.

An extensive survey of the ES and CFS literature reveals that even though many studies characterize and visualize fiber morphology, surprisingly, only a countable few characterize crystallinity, and mechanical properties,<sup>58,67–73</sup> and hardly any present comparisons of centrifugally spun with electrospun fibers. Intrigued, we spun PEO fibers using the CFS setup we designed (as detailed elsewhere<sup>61</sup>) and observed that crystallinity characterized using differential scanning calorimetry (DSC) and mechanical properties characterized using tensile testing for centrifugally spun fibers rival those measured for the electrospun PEO fibers.<sup>62</sup> However, our CFS studies used solutions of PEO in pure acetonitrile (AcN) as a solvent, whereas most of the ES studies utilize spinning dope based on aqueous PEO solutions.<sup>58,68–70,74</sup> Therefore, in this contribution, we characterize the influence of changing the AcN fraction in AcN/H<sub>2</sub>O solvent mixtures on diameter, crystallinity, and mechanical properties of the centrifugally spun PEO fibers using matched macromolecular and processing parameters. Furthermore, we contrast the values of the diameter, % crystallinity, tensile strength, and elongation-at-break of the centrifugally spun PEO fibers against the published values for electrospun fibers. For ordinate, we use the Berry number,  $c[\eta]$ , defined as

the product of polymer concentration,  $c$ , and intrinsic viscosity,  $[\eta]$ , for it is a combined variable that captures the influence of  $c$ ,  $M_w$ , and solvent quality. We also list the applications of PEO fibers, ranging from drug delivery, antimicrobial filters, battery separators, photovoltaics, and separation membranes for each previous study. In addition to shear flows, fiber spinning involves free surface viscoelastic flows and instabilities and involves stream-wise velocity gradients associated with extensional flows. It is well-established that the knowledge and analysis of shear rheology are inadequate to estimate extensional relaxation time and extensional viscosity. Here, we contrast the extensional rheology response and pinching dynamics of solutions with matched PEO concentration but varied the AcN fraction using dripping-onto-substrate (DoS) rheometry protocols that we developed to overcome many longstanding characterization challenges and elucidate the influence of polymer concentration flexibility, extensibility, segmental dissymmetry, and charge.<sup>29–33,63,75–80</sup>

Even though innumerable studies correlate spinnability with the role of entanglements or rheological response,<sup>8,9,45–48,54,61–63</sup> here, we find that spinnability and fiber morphology are distinct, even though the number of entanglements, degree of chain overlap, and processing conditions were matched for the PEO in AcN/H<sub>2</sub>O mixtures.<sup>63</sup> We recently examined non-Newtonian fluid mechanics underlying fiber spinning, the role of evaporation, macromolecular and solvent-dependent parameters, and processing conditions. We found that all the ES and CFS data sets can be classified into two scenarios we christened as volatile-entangled (VE) and extensibility-enhanced (EE) spinnability. We reasoned that strong viscosity enhancement due to evaporative loss from entangled solutions facilitates fiber formation<sup>63</sup> and argued that PEO solutions formulated in AcN/H<sub>2</sub>O mixtures containing more 50% AcN fraction display VE spinnability. In contrast, we showed that for matched solvent, processing conditions, and polymer concentrations, even unentangled polystyrene (PS) solutions can be centrifugally spun by the inclusion of an ultrahigh molecular weight (UHM<sub>w</sub>) PS (<0.1 by weight fraction) displaying extensibility-enriched (EE) spinnability.<sup>64</sup> In this contribution, we collect and visualize new and published ES and CFS data for PEO solutions on  $c$ - $M_w$  plots for systems with VE spinnability. We list examples of EE spinnability for fibers spun by the inclusion of PEO as a UHM polymeric additive in a low weight fraction to facilitate fiber formation from formulations containing particles, proteins, or lower  $M_w$  and extensibility polymers or formulations deemed not spinnable.<sup>63,64</sup> We anticipate that our characterizations and comparisons of polymer solution spinnability, and subsequent fiber morphology and properties, present crucial steps toward establishing the algorithm of choices and parameters for synthesis, rheology, processing, and morphology for manufacturing fibers at lower costs, higher production rate, and application-specific properties.

## EXPERIMENTAL METHODS AND MATERIALS

**Spinning Dope Preparation and Parameters Used for Centrifugal Fiber Spinning.** PEO of molecular weight,  $M_w = 600$  kg/mol (Sigma-Aldrich), was dissolved in solvent mixtures containing deionized water (H<sub>2</sub>O) and AcN solvent (high-performance liquid chromatography grade, VWR chemicals). As flexible polymers are prone to chain scission, mild mixing conditions were employed, and no change in the molecular weight was observed before and after mixing. We centrifugally spun PEO fibers from spinning dopes prepared in AcN/H<sub>2</sub>O solvent mixtures using matched processing parameters

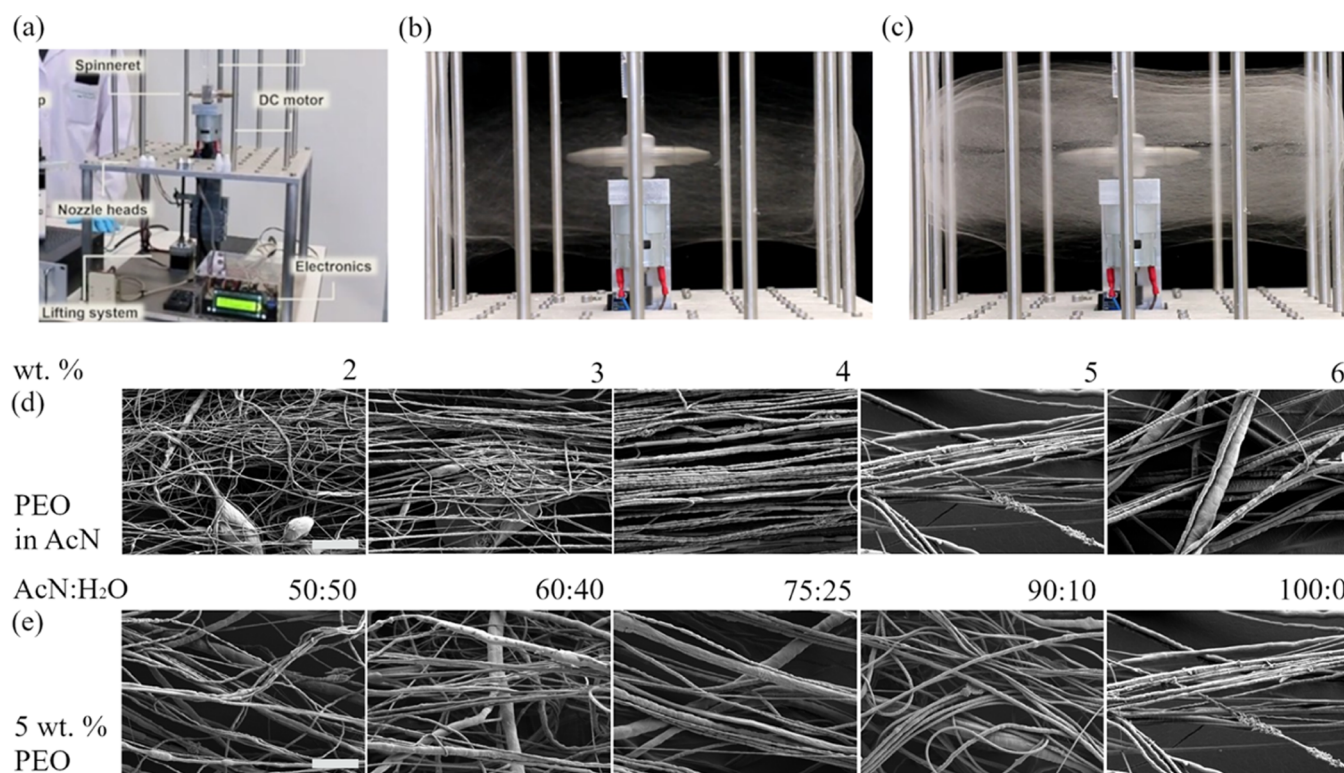


**Figure 1.** CFS of PEO fiber mats from AcN/H<sub>2</sub>O mixtures. (a) Photograph of the home-built CFS or rotary jet spinning setup. The labels mark the critical parts of the apparatus including an injector, a spinneret, a DC motor, and the electronics that allow control over the rotational speed. (b) Snapshot showing the fiber spinning process that deposits continuous fibers (CFs) on the collectors. (c) Example of fiber mat, formed with the collected fibers. (d) SEM images of fibers centrifugally spun from solutions formed in pure AcN as a solvent show a transition from beaded fibers (BF) to CFs occurs on increasing PEO concentration (shown in wt %). (e) SEM images for fibers spun from 5 wt % PEO solution as a function of AcN fraction. The scale bar is 20  $\mu\text{m}$ .

including rotational speed (4000 rpm), temperature (298 K), nozzle diameter (0.6 mm), and nozzle–collector distance (12 cm). The bespoke CFS setup that allows the flexibility for changing nozzle type, material, and nozzle–collector distance was detailed in our previous contributions focused on spinnability and properties of PS and PEO fibers.<sup>61–64</sup>

#### Characterization of Fiber Diameter and Thermal Properties.

The fiber diameter and standard deviation were analyzed in ImageJ using scanning electron microscopy (SEM) images acquired with a ZEISS Gemini 450 (Zeiss, Zaventem, Belgium). Images were taken at three random spots on every sample using magnifications of  $\times 250$ ,  $\times 1000$ , and  $\times 4000$ . At least 100 fibers were measured in every sample, evenly divided over the different images. To obtain statistically reliable values, thermal characterization of the fibers <5 mg was performed via DSC measurements on a Q200 instrument (TA Instruments, Assen, Belgium) over a temperature range of 20–150  $^{\circ}\text{C}$ , at a heating/cooling rate of 20  $^{\circ}\text{C}$  per minute.

**Characterization of Shear and Extensional Rheology.** The steady shear viscosity,  $\eta(\dot{\gamma}) \equiv \tau_{12}/\dot{\gamma}$ , was characterized using cone-and-plate geometry (50 mm diameter, 1 $^{\circ}$  cone angle) on an Anton Paar MCR 302 rheometer (torque range  $10^{-5}$  and 200 mN m). Here, the shear stress,  $\tau_{12}$ , in response to imposed shear rates in the range of  $\dot{\gamma} = 0.01\text{--}10^3 \text{ s}^{-1}$  was measured at constant temperature (maintained using a Peltier element). A solvent trap was used to minimize the influence of solvent evaporation on the measurements. We characterized the pinching dynamics, elasticity, and extensional rheology response of the PEO solutions using the closed-cell DoS rheometry. A finite volume of fluid is dispensed at a low and fixed flow rate ( $Q = 0.02 \text{ mL/min}$ ) through a stainless-steel nozzle with outer and inner diameter as  $2R_0 = 2.108 \text{ mm}$  and  $D_i = 1.6 \text{ mm}$ , respectively. The dispensing is stopped when the drop contacts the partially wetting substrate placed at a height  $H$  below the nozzle, thus creating an hour-glass-shaped liquid bridge, with an aspect ratio of  $H/D_0 \approx 3$ . The neck shapes and shape evolution

are visualized using an imaging system that includes a light source, a diffuser, a high-speed camera (Fastcam SA3 with a Nikkor 3.1  $\times$  zoom (18–25 mm) lens), and an attached macro lens to improve magnification. Reasonably high frame rates (8000–25,000 frames per second) were used to obtain a high-quality data set. A closed transparent cell was used to carry out experiments in an atmosphere saturated with solvent vapor to minimize the influence of evaporation. The DoS videos are analyzed with specially written MATLAB codes to determine the minimum neck radius as a function of time. The experimental setup, design considerations, advantages contrasted to other extensional rheology methods, and the various analyzing protocols are detailed in our previous contributions.<sup>29–33,63,76–79</sup>

**Characterization of Mechanical Properties.** Finally, tensile testing was carried out on centrifugally spun fiber mats (60  $\times$  10 mm) collected in an aligned orientation using a Tinius Olsen (SST) apparatus (Redhill, UK) at a speed of 10 mm/min, with a preload of 0.2 N. The fiber samples were mounted into the clamps with a gage length of 20 mm, and the measurements were started. Before measurement, the samples were weighted, and the surface area was calculated via  $\rho = m/V$  and  $A = V/l$ , where  $\rho$  is the density of PEO ( $= 1.12 \text{ g/cm}^3$ ) and  $m$ ,  $l$ ,  $A$ , and  $V$  are the sample's mass, length, surface area, and volume, respectively. From tensile testing, the Young's modulus and tensile stresses were calculated. For comparison, a rectangular PEO bar was prepared by solvent casting 5 wt % solutions over 2 days and cutting a rectangular 60  $\times$  10 mm section for tensile testing.

## RESULTS AND DISCUSSION

### CFS of PEO Fibers from AcN/Water Solutions.

Centrifugally spun PEO fibers were obtained using the home-built setup that includes two symmetrically mounted nozzles and designed for adjusting collector–nozzle distance by moving pillars or raising the base. Different parts of the setup are labeled

in the photograph included as Figure 1a. Fibers were centrifugally spun with matched processing parameters and similar environmental conditions. Table 1 lists the parameters,

**Table 1. Experimental Parameters for Centrifugal Spinning Setup and Conditions Used in Our Work<sup>a</sup> and Their Range Based on Published Studies**

parameter	name	units	this work	range
nozzle inner diameter	<i>a</i>	m	$6.0 \times 10^{-4}$	$(4-10) \times 10^{-4}$
spinneret radius	$s_0$	m	0.06	0.06–0.08
collector distance	$R_{\text{collector}}$	m	0.12	0.1–0.4
polymer solution exit velocity at the nozzle	$U_{\text{noz}}$	$\text{m}\cdot\text{s}^{-1}$	4	0.3–4
rotation speed	$\Omega$	$\text{rad}\cdot\text{s}^{-1}$	418	210–2100
polymer solution density	$\rho_{\text{noz}}$	$\text{kg}\cdot\text{m}^{-3}$	700–1000	1 000–1 070
polymer solution viscosity at the nozzle	$\mu_{\text{noz}}$	$\text{mPa}\cdot\text{s}$	<100	50–125

<sup>a</sup>Following the nomenclature and definitions outlined in Noorzi et al., we include an asterisk (\*) to identify parameters associated with the surrounding air and subscript noz. to identify viscoelastic jet parameters at the nozzle exit.<sup>81,82</sup>

along with the range used by other researchers.<sup>44,81</sup> Even though the process parameters are matched, the change in solvent contributes to variation in properties such as surface tension, viscosity, volatility and vapor pressure (that determine the evaporation rate), and dielectric constant. The snapshot included as Figure 1b,c shows the fiber formation and deposition process. A relatively high degree of alignment can be observed in the as-produced fiber mats, as shown in Figure 1c. The series of SEM images included in Figure 1d show the morphology of fibers spun from PEO solutions formulated in pure AcN as a solvent, whereas the SEM images in Figure 1e display fibers centrifugally spun from  $c = 5$  wt % as a function of the increasing AcN fraction in AcN/H<sub>2</sub>O mixtures.

The centrifugal spinning of PEO solutions in AcN with  $c < 2$  wt % produced only a spray of droplets, BFs were observed for 2–3 wt %, and CFs for 4–6 wt %, as shown in Figure 1d. Centrifugal forces generated by the chosen processing parameters produce insufficient stress to create continuous jets for polymer concentration beyond 6 wt %. Thus, the spinnability range of PEO/AcN solutions for centrifugal fiber spinning at 4000 rpm lies between 2 and 6 wt %. To evaluate the influence of solvent properties, we formulated PEO solutions in solvent mixtures of AcN/H<sub>2</sub>O ratios of 90:10, 75:25, 60:40, and 50:50. CFs form in the pure AcN solvent and for AcN/H<sub>2</sub>O mixtures up to a 60:40 solvent composition. However, the 50:50

composition showed the initiation of bead formation in the fiber mat. The fiber diameters are comparable for the 90:10 and 75:25 solvent compositions and again a decrease was observed for the 60:40 and 50:50 compositions. For solvent, mixtures with water content higher than 50% were used, no fibers formed, and only bead formation was observed for both concentrations. An increase in the fraction of AcN appears to favor fiber formation. Comparison of surface tension and viscosity values of the solvent as a function of the AcN fraction (see Table 2) shows that increasing AcN leads to a decrease in both viscosity and surface tension. Table 2 also lists the fiber diameters measured for 3 and 5 wt % PEO in different solvent mixtures, and we find that lower polymer concentrations and increased water fraction both lead to a decrease in fiber diameter.

**Shear Rheology of PEO Solutions Formulated in AcN/H<sub>2</sub>O Mixtures.** Steady shear viscosity as a function of shear rate,  $\dot{\gamma}$ , plotted in Figure 2a for 3 wt % PEO solutions shows a Newtonian plateau at a low shear rate followed by shear thinning response. The zero-shear viscosity,  $\eta_0$ , values exhibit higher viscosity values for PEO solutions formulated in pure water than pure AcN solutions. We previously reported that the viscosity values display similar scaling law exponents for these two solvents. The aqueous PEO solutions show  $\eta_0 \propto c^k$  with exponent,  $k = 1, 2,$  and  $4.4$  corresponding to the dilute, semidilute, unentangled, and semidilute, entangled regimes.<sup>83</sup> The entanglement concentration,  $c_e \approx 1.8$  wt %, is also comparable in both solvents. Thus, all PEO solutions used in this study to form fibers lie in the entangled regime. A comparison of relative viscosity values obtained for 3 and 5 wt % PEO solutions showcases that in the entangled regime, increasing polymer concentration provides a dramatic increase in viscosity.

**Pinching Dynamics and Extensional Rheology Response.** We carried out an investigation of the pinching dynamics and extensional rheology response using DoS rheometry. The PEO solutions in AcN/H<sub>2</sub>O mixtures display a longer filament lifespan,  $t_f$ , despite a lower shear viscosity. The radius evolution plots show an initial viscocapillary (VC) response with a linear decrease in neck radius, followed by an elastocapillary (EC) regime that shows an exponentially slow decay in the radius. The EC regime attributed to the interplay of capillarity, and nonlinear viscoelastic stresses arise in response to extensional flows within pinching necks. Our previous studies describe the development and interpretations of the various expressions used to describe the EC regime.<sup>29–32,76</sup> Here, we simply note that the data sets were fit using the following modified expression (introduced by Dinic and Sharma<sup>31</sup>):

$$\frac{R(t)}{R_0} = \left( \frac{G_E R_0}{2\sigma} \right)^{1/3} \exp\left( -\frac{t - t_c}{3\lambda_E} \right) \quad (1)$$

**Table 2. Experimentally Determined Values of Surface Tension and Viscosity for Various Solvent Mixtures, the Zero-Shear Viscosity ( $\eta_0$ ) and the Calculated Relative Viscosity of the PEO Solutions, and the Fiber Diameter ( $d_f$ ) (and Its Standard Deviation) Determined by Analyzing Three SEM Images and Taking an Average of at least 100 Fiber Diameters**

solvent properties			3 wt %			5 wt %		
$\Phi_{\text{AcN}}$ [-]	$\sigma$ [ $\text{mN}\cdot\text{m}^{-1}$ ]	$\eta_s$ [ $\text{Pa}\cdot\text{s}$ ]	$\eta_0$ [ $\text{Pa}\cdot\text{s}$ ]	$\eta_r$ [-]	$d_f$ [ $\mu\text{m}$ ]	$\eta_0$ [ $\text{Pa}\cdot\text{s}$ ]	$\eta_r$ [-]	$d_f$ [ $\mu\text{m}$ ]
100	34	0.00036	0.1	278	$0.7 \pm 0.3$	1.06	2944	$1.6 \pm 0.8$
90	35	0.00039	0.085	218	$0.7 \pm 0.4$	0.83	2128	$1.6 \pm 1.0$
75	34	0.00051	0.12	235	$0.7 \pm 0.8$	1.13	2216	$1.7 \pm 1.2$
60	34	0.00069	0.27	391	$0.6 \pm 0.3$	2.61	3783	$1.5 \pm 1.1$
50	34	0.00076	0.36	474	$0.5 \pm 0.2$	3.42	4500	$1.4 \pm 1.0$

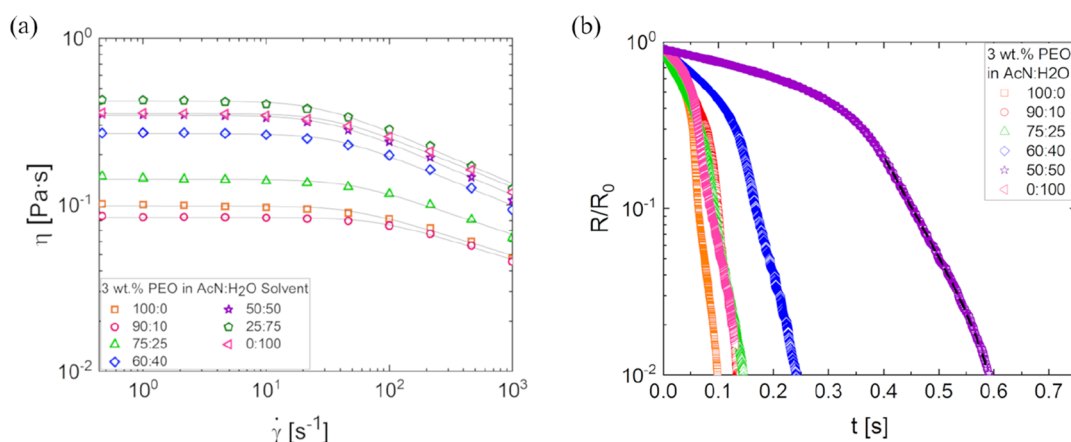


**Figure 2.** Shear and extensional rheology of PEO in AcN-Water mixtures. (a) Steady shear viscosity data as a function of shear rate show that the 3 wt % PEO solutions exhibit shear thinning for all solvent mixtures. The onset of shear thinning that provides a measure of shear relaxation time appears nearly matched. (b) Radius evolution data plotted as a function of time is obtained from the image analysis of pinching necks. The self-thinning of the neck is visualized and captured using closed-cell DoS rheometry. Dashed lines show the elastocapillary (EC) regime that can be discerned for the 3 wt % PEO solutions formulated in a different solvent. The variation in filament lifespan as a function of the AcN fraction is not directly correlated with shear rheology response. The EC fits yield comparable extensional relaxation time values for the solutions shown.

**Table 3. Time Scales and Dimensionless Groups That Capture the Measured Variation in the Rheological Response and Pinching Dynamics of 3 wt % PEO as a Function of AcN Fraction**

solvent		3 wt % PEO							
$\phi_{\text{AcN}}$ [-]	$\sigma$ [N/m]	$\eta_0$ [Pa·s]	$\lambda_s$ [s]	$\lambda_E$ [s]	$t_f$ [s]	$Ca$ [-]	$Oh$ [-]	$Wi$ [-]	
100	0.034	0.1	0.03	0.0041	0.082	0.09	1.03	1.5	
90	0.035	0.085	0.017	0.00335	0.14	0.07	0.87	0.85	
75	0.034	0.12	0.017	0.0035	0.15	0.10	1.23	0.85	
60	0.034	0.27	0.026	0.013	0.26	0.23	2.78	1.3	
50	0.034	0.36	0.037	0.022	1.1	0.31	3.70	1.85	

Here,  $t_c$  refers to the onset of EC,  $G_E$  computes an apparent extensional modulus, distinct from the corresponding shear values, and, likewise,  $\lambda_E$  refers to the extensional relaxation time.<sup>29–32</sup> Although the shear viscosity, shear relaxation time, and extensional relaxation time (discussed later) are almost comparable for the range of PEO solutions (see Table 3), only solvent mixtures with >50% AcN lead to the formation of fibers due to faster evaporation.<sup>63</sup> The radius evolution data show a longer filament lifespan for the intermediate AcN concentrations. Even though shear viscosity too is higher in AcN/H<sub>2</sub>O mixtures than in pure AcN and H<sub>2</sub>O, the values peak at a different composition. The variation in hydrogen-bonding interactions in mixed solvents influences polymer conformation and manifests in rheological measurements.<sup>84</sup> Fiber spinning involves evaporative loss of solvent, with associated changes in interchain overlap and interactions, and a rather complex deformation history that are likely to influence the chain conformations and crystallinity and mechanical properties of resulting fibers, as explored in the next subsection.

The growth of sinusoidal instability and pinching dynamics of necks of viscous fluids depends on the interplay of viscous stress and capillary pressure. For Newtonian viscous fluids, the characteristic time known as the VC time,  $t_{vc} = \eta_0 D_0 / \sigma$ , governs the pinching dynamics, whereas for low viscosity fluids, dynamics are governed by an interplay of inertia and capillarity, leading to inertio-capillary time,  $t_{ic} = \sqrt{\rho R_0^3 / \sigma}$ . The dimensionless viscosity, expressed as Ohnesorge number,  $Oh = \eta / \sqrt{\rho \sigma D_0}$  equals to the ratio of VC time,  $t_{vc}$  to inertio-capillary time,  $t_{ic}$ .<sup>85,86</sup> Electrospinnability and more recently CFS spinnability are often

attributed to the role played by entanglements or topological constraints<sup>8,9,46–48,54,61–63</sup> and usually linear viscoelastic measures such as zero shear viscosity are used for identifying spinnable solutions. Ren et al.<sup>45</sup> constructed an “operating diagram” using a plot of  $Oh$  against a Weissenberg number,  $Wi = \lambda_s \dot{\gamma}$  (compares shear relaxation time to the time scale equal to the inverse of deformation rate). Ren et al.<sup>45</sup> argued that maps can be drawn using Ohnesorge number,  $Oh = \eta_0 / \sqrt{\rho \sigma D_0}$ , against a Capillary number  $Ca = t_{vc} / t_{cent}$  such that  $t_{cent} = R_0 / U_{cent}$  depends on centrifugal speed.<sup>45</sup>

As polymer solution viscosity increases with a strong power law exponent ( $k = 4.4$ ) in the entangled regime, the values of parameters such as  $Oh$ ,  $Ca$ , and  $Wi$  rise significantly in the entangled regime. However, our experimental results show that spinnability is quite different even if shear viscosity, relaxation time, and RPM are nearly matched, implying that the location on  $Wi-Oh$  or  $Ca-Oh$  diagrams is not sufficient for evaluating spinnability as a function of solvent choice. As free surface flows associated with fiber formation invariably involve nonlinear deformation and stream-wise velocity gradients associated with extensional rheology response, the utility of such  $Oh-Ca$  or the  $c-M_w$  processability maps is limited by the inadequate accounting for the influence of elasticity and rate- or concentration-dependent extensional rheology response that is not linearly correlated with the corresponding shear rheology response. The dimensionless measures of viscous contribution,  $Ca$  and  $Oh$ , computed for 3 wt % PEO increase with the water fraction (see Table 3). For any solvent, the  $Ca$  and  $Oh$  values increase by over an order of magnitude as PEO concentration

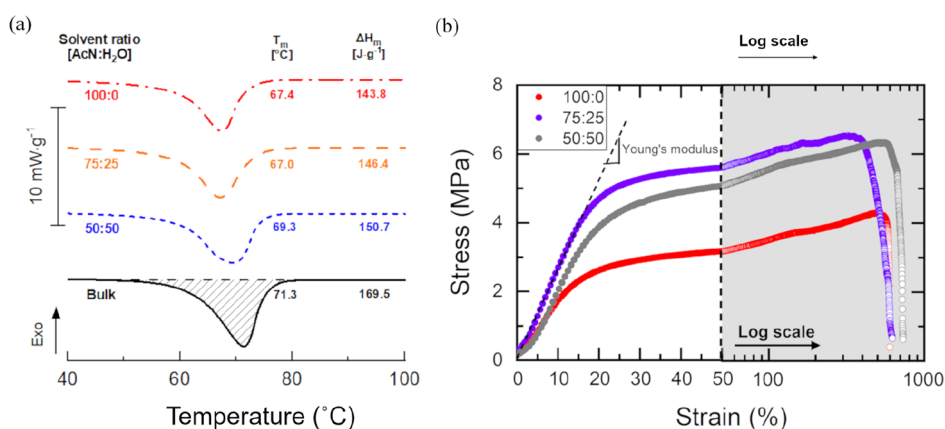


**Figure 3.** Thermal and mechanical properties of the centrifugally spun fiber mats. (a) DSC thermograms of the spun fiber mats. Here, the heating curves show the difference in crystallinity and melting peak for the fibers spun from different concentrations of PEO in AcN. A bulk PEO sample (powder) is included for comparison. The temperature was varied between 20 and 150 °C, at a heating/cooling rate of 20 °C per minute. (b) Mechanical properties of fiber mats centrifugally spun from 5 wt % PEO using varied solvent composition. The low strain region uses a linear scale, whereas the shaded region uses a logarithmic scale.

increases from 3 to 5 wt %. In Ren et al.,<sup>45</sup> higher  $Ca$  and  $Oh$  values were associated with spinnability, and thus, better fiber formation would be expected for higher  $Ca$ , higher  $Oh$  aqueous solutions, contrary to the observations here. We recently detailed the influence of evaporation and rheology on centrifugal spinning and created processability diagrams that incorporate the critical influence of evaporation time (proportional to or measured by thermogravimetric analysis).<sup>63</sup>

#### Thermal Properties of Centrifugally Spun PEO Fibers.

The DSC curves of the PEO fibers spun using solvent mixtures with varied AcN/H<sub>2</sub>O ratios included in Figure 3a provide a measurement of the melting temperature,  $T_{m,1}$ , and the enthalpy of crystalline melting,  $\Delta H_m$ . The enthalpy, computed by integrating the area under the melting peak, as displayed for the bulk sample can be used for computing crystallinity,  $X_c$ , via

$$X_c = \frac{\Delta H_m}{\Delta H_m^*} \times 100\% \quad (2)$$

Here,  $\Delta H_m^*$  is the melting enthalpy for pure crystalline PEO and has a value of 213.7 J/g.<sup>87,88</sup> We find that an increase in the H<sub>2</sub>O content in the solvent leads to an increasing melting enthalpy and higher crystallinity. Furthermore, the melting peak slightly increases from 67.4 °C (pure AcN) toward 69.3 °C (solvent ratio 50:50). The fiber crystallinity and microstructure can be expected to show some variation due to solvent-influenced differences in evolution of polymer conformation and viscoelastic stresses.<sup>89</sup> Also, the longer evaporation rate for the aqueous solvent mixtures will increase the crystal growth time in the fibers. All numerical values for the thermal analysis of the fiber mats are displayed in Table 4.

**Mechanical Properties of PEO Solutions Centrifugally Spun from AcN/H<sub>2</sub>O Mixtures.** The stress–strain curves via tensile testing of 6 cm-long fiber mats are included in Figure 3b. The slope of the stress–strain curve in the low strain limit provides a measurement of Young's modulus, whereas the peak value quantifies the tensile strength, and the area under the curve signifies toughness. The linear  $x$ -axis is used for the low strain to clearly show variation in Young's modulus, and the logarithmic axis is included at high strain, to highlight the value of large extension at break. Bulk PEO samples show a yield point, followed by strain hardening upon higher extension. However, the yield point is not observed for the fibrous samples. Table 5

**Table 4.** Melt Temperature of the First ( $T_{m,1}$ ) and Second ( $T_{m,2}$ ) Heating Curve, Melting Enthalpy ( $\Delta H_m$ ), and the Crystallinity ( $X_c$ ) of the PEO Bulk Material and the Fiber Mats Spun from Different Concentrations in AcN

solvent (AcN/H <sub>2</sub> O)	sample	$T_{m,1}$ [°C]	$T_{m,2}$ [°C]	$\Delta H_m$ [J/g]	$X_c$ [%]
	Bulk	71.3	66.86	169.5	79.3
100:0	3 wt %	66.9	68.27	135.0	63.7
	5 wt %	67.4	67.67	143.8	67.3
75:25	5 wt %	67.0	67.47	146.4	68.5
50:50	5 wt %	69.3	67.69	150.7	70.5

lists the four mechanical properties determined from the analysis of the measurements included in Figure 3b. The comparison of the mechanical response of fiber samples spun from 5 wt % PEO in different solvent compositions shows that the increasing water fraction in the solvent leads to stronger fiber mats (Figure 3b). The properties reported here are all measured using fiber mats obtained in a relatively high degree of orientation from our bespoke setup and are all formed under similar processing conditions.

Based on our experiments and the published literature, we anticipate that processing conditions and formulation properties (solvent choice, polymer concentration, and molecular weight) impact the fiber diameter, crystallinity, and mechanical properties. However, from the perspective of picking polymeric fibers for a particular application, it is important to consider the range of diameters, crystallinity, and mechanical properties that can be attained for chosen materials. With this underlying motivation, we previously tabulated mechanical properties of PEO fibers made using pure AcN and determined that centrifugally spun PEO fibers rival properties of electrospun PEO fibers typically made from aqueous PEO solutions as a spinning dope.<sup>62</sup> In Figure 4, we contrast the diameter, Young's modulus, tensile strength, and extension at break for centrifugally spun PEO fibers (this study) with the literature data for electrospun PEO fibers.<sup>45,58,68–73,90–93</sup> By ascribing distinct symbols for data sets extracted from published studies in Figure 4, we emphasize that only a few measurements exist, and a more systematic study is warranted for connecting properties to macromolecular properties and processing parameters. Here, we utilize Berry number,  $c[\eta]$  (also called overlap parameter), as a combined variable on

Table 5. Mechanical Properties of the Centrifugally Spun PEO Fiber Mats

solvent [AcN/ $\text{H}_2\text{O}$ ]	PEO conc. [wt %]	tensile strength [MPa]	Young's modulus [MPa]	elongation-at-break [-]	fiber toughness [ $\text{kJ}\cdot\text{m}^{-3}$ ]
100:0	3	$1.80 \pm 0.72$	$4.88 \pm 0.72$	$445.9 \pm 62.5$	$695 \pm 95$
	5	$4.23 \pm 0.76$	$15.3 \pm 2.14$	$517.5 \pm 78.2$	$1897 \pm 499$
75:25	5	$6.16 \pm 0.66$	$25.42 \pm 1.76$	$681.1 \pm 143.5$	$2924 \pm 322$
50:50	5	6.32	23.68	730.7	$4117 \pm 500$

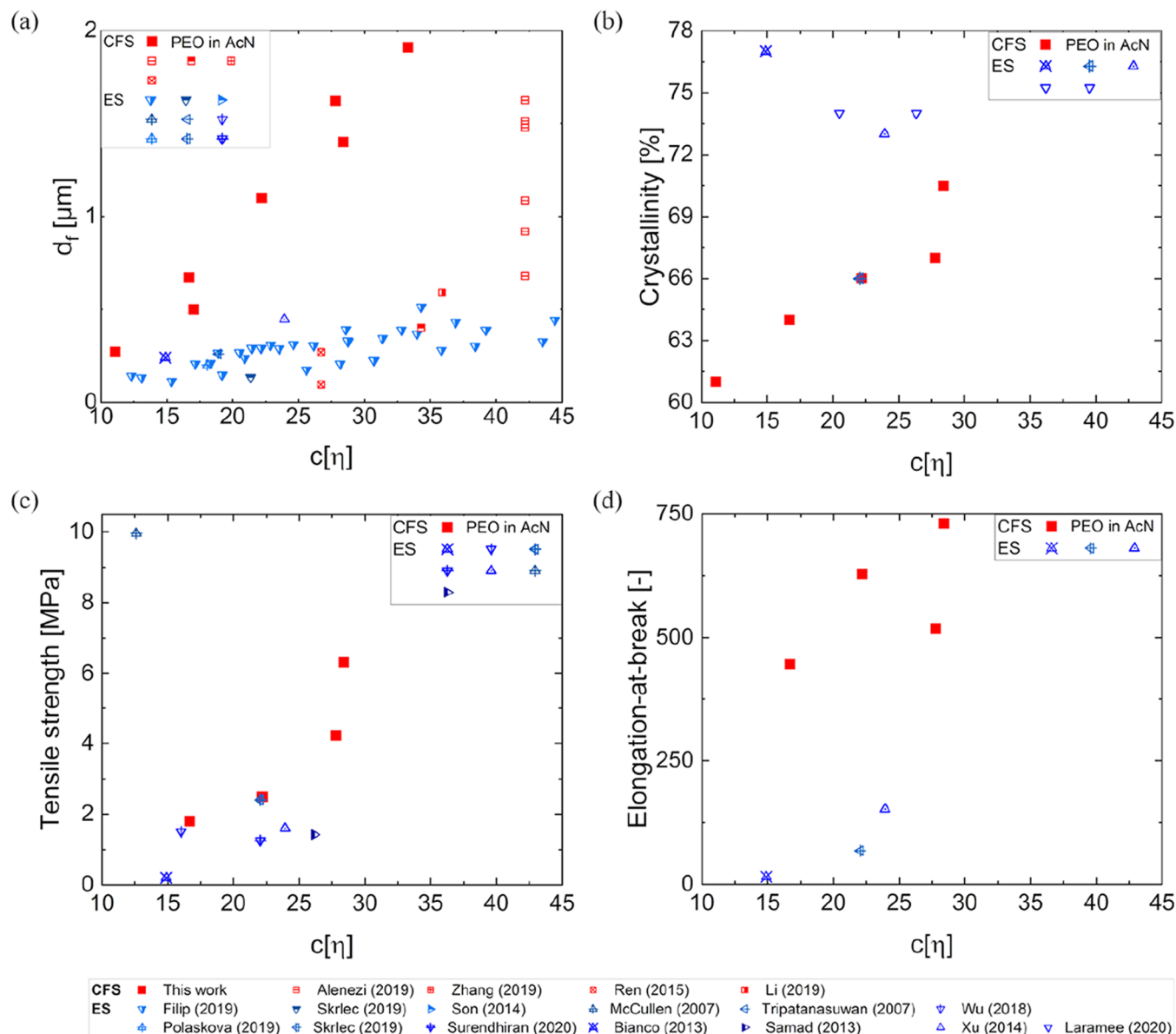


**Figure 4.** Centrifugally spun emulate properties of electrospun fibers. (a) Diameter, (b) crystallinity, (c) tensile strength, and (d) elongation-at-break of the centrifugally spun fiber mats (data shown in red for this study was produced under matched processing conditions) contrasted with the literature values for electrospun PEO fiber mats produced under varied spinning conditions, and a range of molecular weights and solvent types.<sup>45,58,68–73,90–93</sup>

the  $x$ -axis to capture the effect of polymer molecular weight and concentration, as well as solvent quality. Above the entanglement concentration, the increased screening of excluded volume interactions diminishes the difference in static and dynamic properties between good and theta solvents. Hence, the initial chain conformation and orientations are presumably similar for the PEO solutions in solvent mixtures with difference in the AcN fraction. Figure 4 shows that the thermal and mechanical properties, measured for dried, solid PEO fibers, are comparable for electrospun and centrifugally spun fibers, despite differences

in processing parameters, deformation history, and solvent–polymer interactions within the spinning dope.

**PEO  $c$ - $M_w$  Plot, Spinnability, and Applications.** The rationale for considering PEO as a representative polymeric material for exploring the fiber engineering trifecta is further supported by the data included in Figures 4 and 5 and in Tables 6 and 7 that summarize macromolecular properties ( $M_w$  and  $c$ ), solvent choice, processing parameters, and applications of electrospun and centrifugally spun PEO fibers. For the listed applications that range from drug delivery, antimicrobial filters,

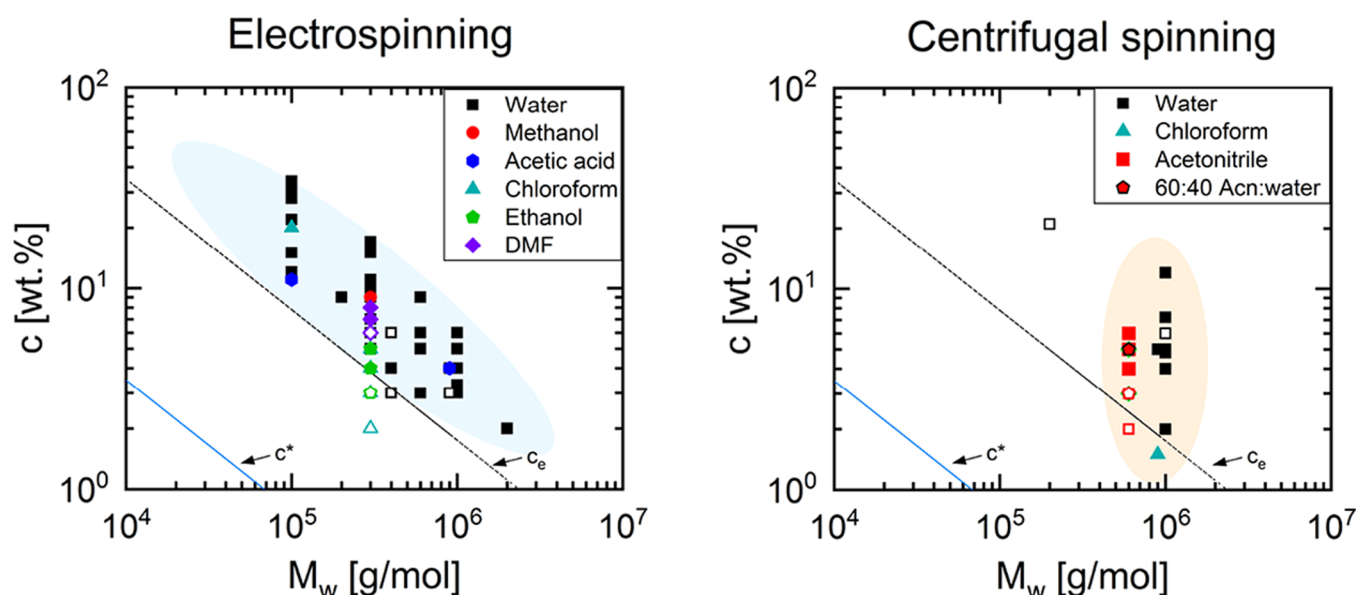


**Figure 5.** VE spinnability of PEO solutions in various solvents. On the  $c$ - $M_w$  plot, the beaded and CFs are shown in open and closed symbols, respectively. The dotted blue line shows the overlap concentration,  $c^*$ , whereas the black dash-dotted line corresponds to the  $10c^*$  to indicate concentrations beyond which entanglements play a role. A much more extensive range of polymer molecular weights and concentrations was explored in ES experiments. Tables 6 and 7 summarize the details about processing parameters, molecular weight and concentration ranges, and solvents used in the ES and CFS studies.

battery separators, photovoltaics to separation membranes, PEO is either present as the primary fiber former that manifests VE spinnability or as a stringiness facilitator, as an additive that enables fiber formation due to extensibility-enhanced spinnability. In VE PEO solutions, the substantial concentration-dependent rise in viscosity on evaporation stabilizes the jet against capillarity-driven growth in sinusoidal instability and break-up leading to fiber formation.

Increasing polymer molecular weight or concentration changes both the solution viscosity and viscoelasticity and both impact the onset and growth of surface-tension-driven instabilities that lead to the formation of sinusoidal perturbations of jets.<sup>27,85,86</sup> The formation of beads or sprayed drops, beads-on-a-string structures, and CFs is sequentially observed if  $c$  increases for fixed  $M_w$  polymer or  $M_w$  changes for a fixed  $c$ .<sup>45–48,54,61–63</sup> Although the change in the polymer composition is primarily discussed in terms of its impact on the shear rheology (usually zero shear viscosity), profound change can be observed in both linear and nonlinear viscoelastic measures of polymer solutions including relaxation time, relaxation modulus, the first normal stress difference, and extensional viscosity.<sup>26,29–32,76</sup> However, as the entangled solutions display shear thinning at high deformation rates and extensional thinning at intermediate rates associated with fiber spinning, it is likely that viscosity enhancement due to evaporative loss of solvent plays a more significant role than strain hardening or delayed pinching flows due to high extensional viscosity. We posit that equilibrium properties such as the number of entanglements, zero shear viscosity or shear relaxation time can be used for identifying this VE spinnability in many polymeric systems. However, in applications that rely on the use of UHM PEO, the improved spinnability must be attributed to the significant delay in a capillarity-driven pinching for the high extensibility, high extensional viscosity, strain hardening PEO, in comparison with polysaccharide solutions, or dispersions containing particles, proteins, or reactive mono-

mers.<sup>8,9,15,22,28,59,68,69</sup> We refer to these cases as examples of EE spinnability, and these are highlighted in the two tables by showing data sets using the gray font. The table for ES includes only representative data sets, for many more examples that can be found for both VE and EE spinnability; the CFS table represents the current state-of-the-art.

Tables 6 and 7 show that a broader range of PEO molecular weights has been explored using ES than employed for CFS. Electrospinnability and more recently CFS spinnability are often attributed to the role of entanglements, that is, the topological constraints<sup>8,9,46–48,54,61–63</sup> that arise in solutions (and melts) above entanglement concentration,  $c_e$  (and beyond entanglement molecular weight,  $M_e$ ). Hence, the spinnability or processability diagrams are presented with molecular weight,  $M_w$ , and concentration,  $c$ , as the coordinates. The value of  $c_e$  for most flexible, uncharged polymers is typically 5–10 times overlap concentration or  $c^*$ , the concentration above which polymer coils just begin to overlap and shear viscosity of the polymer solution becomes nearly twice that of solvent. As  $c^* = 1/[\eta]$ , and the change in intrinsic viscosity can be estimated using the Mark–Houwink–Sakurada equation,  $[\eta] = KM^a$ , with constant,  $K$ , and exponent,  $a$  (that depends on solvent quality), using the tabulated values for most polymer–solvent pairs, one can estimate  $c_e/c^* \approx N_e^a$ .<sup>83</sup> We envision that lower molecular weight or less extensible or even less polydisperse polymers display spinnability and CF formation for highly entangled solutions not only due to higher viscosity and elasticity compared to unentangled systems but also due to a steep viscosity rise on solvent loss. Rheological measurements carried out using entangled polymer solutions at a fixed concentration display pronounced shear thinning and extensional thinning at intermediate rates,<sup>103–105</sup> and therefore, we anticipate that strong viscosity enhancement on solvent evaporation is needed to compensate for any strain-softening.

We present the data sets cited in Tables 6 and 7 for fiber spinning from PEO solutions on the  $c$ - $M_w$  plot in Figure 5 and



Table 6. Solvent, Polymer Molecular Weight and Concentration, Zero Shear Viscosity, Spinning Conditions (Voltage), and Fiber Morphology and Diameter Are Tabulated If Mentioned in the Reference<sup>a</sup>

Solvent / $M_w$	Conc. $c$	Viscosity $\eta$	Voltage $V$	Type/ $d_f$	Spinnability & Applications
kDa	wt. %	mPa·s	kV	nm	
H <sub>2</sub> O / 300	7	215	13	CF	Process and solvent choice
H <sub>2</sub> O / 400	4	/	/	CF	Role of entanglements <sup>48</sup>
H <sub>2</sub> O / 2 000	< 2	/	/	CF	
H <sub>2</sub> O / 400	3	/	5	BF	Electrically conducting fibers <sup>93</sup>
	4	≈ 200		CF	
H <sub>2</sub> O / 400	6	/	5	BF / 63 – 103 CF / 130 – 253	Evaporation rate & controlled RH
H <sub>2</sub> O / 300	10	/	20	CF / 300 – 2000	Electrochemical device <sup>69</sup>
H <sub>2</sub> O / 100	15	≈ 200	12	CF / 240	Mechanical properties of PEO/PHBV blend fibers <sup>68</sup>
H <sub>2</sub> O / 1 000	4	≈ 1 600	12	CF / 446	Reinforcement of PEO nanofibers
H <sub>2</sub> O / 600	5	/	/	BF CF	Extensibility-enriched spinnability <sup>94</sup>
50% AA / 600	/	/	/	/	CS/PEO nanofibers; reducing bacterial growth on foods <sup>17</sup>
50% AA / 900	/	/	/	CF	CS/PEO fibers for reducing bacteria in foods <sup>18</sup>
H <sub>2</sub> O / 900	3	≈ 800	15	BF	Cellulose nanocrystal rich PEO fibers <sup>88</sup>
H <sub>2</sub> O / 300	9	5.4	25	CF / 200	Thermal treatment influences crystallinity of PEO fibers <sup>72</sup>
MeOH / 300		1.3		CF / 768	
H <sub>2</sub> O / 900	4	≈ 1 300	15	CF	Nanofibers for high loading & long-term viability of probiotics <sup>92</sup>
Aqueous AA / 400	/	/	10 – 12	CF	Local antibiotic delivery systems via chitosan-PEO fibers <sup>95</sup>
AA 2:1 FA / 100	11	≈ 800	15	CF	PEO/PCL blends, functionalized for protein attachment <sup>96</sup>
2% AA / 900	4	189	20	CF / 227	PEO with chitosan and PE for the reduction of E. Coli population <sup>71</sup>

<sup>a</sup>The fiber morphology is either BFs or CFs. Solvent names are abbreviated: acetic acid, formic acid (FA), and ethyl acetate (EA). Entries in light gray shade show EE spinnability.

include overlap concentration,  $c^*$ , and entanglement concentration,  $c_e \approx 10c^*$ , as slanted line for aqueous solutions. Here, we include the studies for unblended PEO fibers only and thus plot includes data sets that correspond to VE spinnability. It is evident that both ES and CFS display spinnability for entangled polymer solutions formulated in a wide range of solvents, and the molecular weights and concentrations that lead to the CF formation cluster together on the  $c$ - $M_w$  plot despite the differences in the processing parameters and driving forces. Although most of the CFS studies used higher  $M_w$  polymers, Alenezi et al.<sup>99</sup> centrifugally spun CFs from aqueous solutions of 200 kDa PEO by utilizing relatively high concentrations (21 wt %) and using rather high rotational speed (8500–10,000

rpm).<sup>99</sup> Recently, Müller et al.<sup>13</sup> spun PEO fibers using electrocentrifugal spinning and reported that on dropping  $M_w$  from 100 to 35 kg/mol, transition from continuous to BFs is observed even if the PEO concentration is increased from 200 to 500 g/l, whereas 500 g/l of  $M_w = 20$  kg/mol leads to drops or beads only. We anticipate that future experiments will enlighten us if centrifugal spinning can be carried out with higher concentration PEO solutions ( $c > c_e$ ) for the lower  $M_w$  samples as well, and if needed, blending of a small amount of ultrahigh  $M_w$  PEO could provide the extensibility-enhanced spinnability for PEO-based single polymer, blended or multicomponent composite fibers.

**Table 7. Solvent, Polymer Concentration and Molecular Weight, and Spin Speed Used for Making Centrifugally Spun PEO Fibers, and Fiber Morphology Obtained are Tabulated if Mentioned<sup>a</sup>**

Solvent / Mw (kDa)	Conc. (w%)	Viscosity (mPa·s)	Spin speed (rpm)	Fiber type/ Dia (nm)	Comments
H <sub>2</sub> O	7–16	/	3 000–5 000	CF / 300	CFS process development <sup>35</sup>
CHCl <sub>3</sub> / 900	1.5	/	2 000–5 000	CF / 650	PEO/BEH-PPV hybrid nanofibers <sup>81</sup>
H <sub>2</sub> O / 900	/	/	7 500–9 000	CF	Fiber formation mechanisms
H <sub>2</sub> O / 1000	/	/	5 000	CF	Extensibility-enriched; FeO <sub>2</sub> /PEO fibers <sup>97</sup>
EA / 1000	0.02 (additive)	/	/	/	Extensibility-enriched; UV induced polymerization)
FA:EA /	0.1 (additive)	/	/	/	Extensibility-enriched (parameter research) <sup>19</sup>
H <sub>2</sub> O:NaO H:starch	0.2 (additive)	/	/	/	Extensibility-enriched (EE) spinnability for drug- loaded starch fibers <sup>20</sup>
H <sub>2</sub> O / 1000	4	/	3 000	CF	EE spinnability; tissue eng. alginate/ PEO fiber composites. <sup>98</sup>
H <sub>2</sub> O / 200	21	≈ 3 000	7 000	BF	Simulation of centrifugal spinning compared to pressurized gyration <sup>99</sup>
			8 500–10 000	CF	
H <sub>2</sub> O / 1000	6	178	3 000–5 000	CF / 590	Fabrication of CCS/PEO fibers <sup>100</sup>
H <sub>2</sub> O / 1000	< 2	/	4 000	Beads	Mathematical model for CFS, parametric study <sup>101</sup>
	2–5			BF	
	6			CF / 400	
H <sub>2</sub> O / 1000	4.8–7.2	200 – 4000	/	CF / 1 910 – 3 220	PEO/CMCS composite fibers; wound dressing. <sup>102</sup>
H <sub>2</sub> O / 900	5	/	2 000–20 000	CF	Theoretical model

<sup>a</sup>The fiber morphology is referred to as BFs or CFs. The nonaqueous solvents are abbreviated as follows: acetic acid, formic acid (FA), and ethyl acetate (EA). Entries in light gray shade show EE spinnability.

The comprehensive summary of many data sets included in Figures 4 and 5 provides an unprecedented exploration of the fiber engineering trifecta of spinnability, morphology, and properties for centrifugally spun and electrospun PEO fibers. In addition to highlighting progress and the current state-of-the-art understanding, the discussion and analysis included here are expected to germinate and bring to focus several questions. For example, carrying out a similar survey for more polymers will help us to determine the universal features of spinnability–rheology–volatility–extensibility relationship and significance of tuning shear and extensional rheology and processing parameters. It is possible that the connection between spinnability and rheology and processing behavior of PEO solutions would be the most suitable guide for high flexibility and high extensibility polymers, whereas fiber morphology and properties of PEO would inform better about semicrystalline polymers. Even for PEO, the lower-molecular-weight regime remains relatively unexplored using CFS and could be used for producing fibers by increasing concentration (VE spinnability) or addition of a small weight fraction of the ultrahigh  $M_w$  additive.<sup>64</sup>

## CONCLUSIONS

We show that PEO fibers with crystallinity and mechanical properties comparable to electrospun fibers can be centrifugally spun using VE solutions formulated in AcN–water mixtures as a solvent. Fibers form only for AcN fractions above 50%, although we chose matched macromolecular parameters ( $c$  and  $M_w$ ) and matched processing conditions, including rotational speed (4000 rpm), nozzle type/size/material, and nozzle–collector distance on a bespoke CFS setup. Even though spinnability was observed only for AcN fractions greater than 50%, we found that the crystallinity, measured using DSC, and mechanical properties including tensile strength and elongation at break were enhanced for fibers spun from spinning dope formulated with a higher water fraction. A slower evaporation rate and an increase in the time available for crystallization possibly lead to the observed enhancements. We include qualitative comparisons between the measured diameter, crystallinity, and mechanical properties of centrifugally spun and electrospun fibers by plotting measured values as a function of Berry number, that is, the dimensionless product of concentration and intrinsic viscosity. Even though processing conditions and the mecha-

nism underlying ES and CFS are quite distinct, the qualitative comparison suggests that remarkable similarity exists in the microstructure and elastic properties of solidified electrospun and centrifugally spun fibers.

Finally, to explore the spinnability questions, we compile the spinning dope properties (concentration,  $c$ , and molecular weight,  $M_w$ ) and processing parameters for PEO solutions in various solvents that exhibit electrospinnability and contrast these with PEO solutions found to be centrifugally spinnable. We classify representative examples of ES and nearly all the CFS studies of PEO-based fibers into two categories: VE spinnability if PEO is the only polymer present and EE spinnability for cases with fiber spinning facilitated by high-molecular-weight PEO additive that is blended with a matrix material such as lower  $M_w$  PEO or with other polymers, particles, or proteins. The comprehensive comparison of PEO concentrations and molecular weights that display VE spinnability reveals that published CFS studies relied only on higher  $M_w$  systems (>600 kg/mol). We envision that increasing concentration beyond entanglement concentration (VE spinnability) or the addition of a small weight fraction of the ultrahigh  $M_w$  additive to unentangled solutions (EE spinnability) could present opportunities for producing fibers from PEO of lower  $M_w$  (<600 kg/mol). Additional investigations of ES and CFS polymers are needed and underway to connect polymer physics (macro-molecular properties in solution set by choice of polymer and solvent), shear and extensional rheology, viscoelastic instabilities, processing conditions, morphology, and spinnability. We anticipate that our classification and characterization will inspire future studies on creating thinner, stronger, and more application-ready fibers, with a broader range of molecular weights and concentrations employed in CFS.

## AUTHOR INFORMATION

### Corresponding Authors

**Naveen K. Reddy** – Institute for Materials Research (IMO-IMOMECE), Hasselt University, Diepenbeek B-3590, Belgium; IMEC vzw—Division IMOMECE, Diepenbeek B-3590, Belgium; [orcid.org/0000-0003-0163-485X](https://orcid.org/0000-0003-0163-485X); Email: [naveen.reddy@uhasselt.be](mailto:naveen.reddy@uhasselt.be)

**Vivek Sharma** – Department of Chemical Engineering, University of Illinois at Chicago, Chicago, Illinois 60608, United States; [orcid.org/0000-0003-1152-1285](https://orcid.org/0000-0003-1152-1285); Email: [viveks@uic.edu](mailto:viveks@uic.edu)

### Authors

**Jorgo Merchiers** – Institute for Materials Research (IMO-IMOMECE), Hasselt University, Diepenbeek B-3590, Belgium; IMEC vzw—Division IMOMECE, Diepenbeek B-3590, Belgium

**Cheryl Lynn Slykas** – Department of Chemical Engineering, University of Illinois at Chicago, Chicago, Illinois 60608, United States

**Carina D. V. Martínez Narváez** – Department of Chemical Engineering, University of Illinois at Chicago, Chicago, Illinois 60608, United States; [orcid.org/0000-0002-2356-7208](https://orcid.org/0000-0002-2356-7208)

**Mieke Buntinx** – Institute for Materials Research (IMO-IMOMECE), Hasselt University, Diepenbeek B-3590, Belgium; IMEC vzw—Division IMOMECE, Diepenbeek B-3590, Belgium

**Wim Deferme** – Institute for Materials Research (IMO-IMOMECE), Hasselt University, Diepenbeek B-3590, Belgium; IMEC vzw—Division IMOMECE, Diepenbeek B-3590, Belgium; [orcid.org/0000-0002-8982-959X](https://orcid.org/0000-0002-8982-959X)

**Roos Peeters** – Institute for Materials Research (IMO-IMOMECE), Hasselt University, Diepenbeek B-3590, Belgium

Complete contact information is available at:  
<https://pubs.acs.org/10.1021/acsapm.1c01865>

### Author Contributions

J.M. and C.L.S. contributed equally

### Notes

The authors declare no competing financial interest.

## ACKNOWLEDGMENTS

The authors (J.M. and N.R.) acknowledge IMO-IMOMECE at the University of Hasselt for providing financial support. CM would like to acknowledge funding support by the PPG Industries and CS Teaching Assistantship in the Department of Chemical Engineering at UIC. The Packaging Technology Center is acknowledged for providing access to the tensile testing machine, Dr. Wouter Marchal for access to the DSC apparatus, and Dr. Jan D'Haen for access to SEM.

## REFERENCES

- (1) Gupta, V. B.; Kothari, V. K. *Manufactured Fiber Technology*; Chapman & Hall: London, 1997.
- (2) Ziabicki, A. *Fundamentals of Fibre Formation*; John Wiley & Sons: New York, 1976.
- (3) Li, D.; Xia, Y. Electrospinning of nanofibers: reinventing the wheel? *Adv. Mater.* **2004**, *16*, 1151–1170.
- (4) Park, J. H.; Rutledge, G. C. 50th anniversary perspective: advanced polymer fibers: high performance and ultrafine. *Macromolecules* **2017**, *50*, 5627–5642.
- (5) Barhoum, A.; Pal, K.; Rahier, H.; Uludag, H.; Kim, I. S.; Bechelany, M. Nanofibers as new-generation materials: from spinning and nanospinning fabrication techniques to emerging applications. *Appl. Mater. Today* **2019**, *17*, 1–35.
- (6) Atıcı, B.; Ünlü, C. H.; Yanılmaz, M. A review on centrifugally spun fibers and their applications. *Polym. Rev.* **2021**, 1–64.
- (7) Rogalski, J. J.; Bastiaansen, C. W. M.; Peijs, T. Rotary jet spinning review—a potential high yield future for polymer nanofibers. *Nanocomposites* **2017**, *3*, 97–121.
- (8) Venugopal, J.; Ramakrishna, S. Applications of polymer nanofibers in biomedicine and biotechnology. *Appl. Biochem. Biotechnol.* **2005**, *125*, 147–158.
- (9) Pham, Q. P.; Sharma, U.; Mikos, A. G. Electrospinning of polymeric nanofibers for tissue engineering applications: a review. *Tissue Eng.* **2006**, *12*, 1197–1211.
- (10) Santos, D. M. D.; Correa, D. S.; Medeiros, E. S.; Oliveira, J. E.; Mattoso, L. H. C. Advances in functional polymer nanofibers: From spinning fabrication techniques to recent biomedical applications. *ACS Appl. Mater. Interfaces* **2020**, *12*, 45673–45701.
- (11) Filatov, Y.; Budyka, A.; Kirichenko, V., Electrospinning of Micro- and Nanofibers: Fundamentals in Separation and Filtration Processes. **2007**; Vol. 3, p 488.
- (12) Yoon, K.; Hsiao, B. S.; Chu, B. Functional nanofibers for environmental applications. *J. Mater. Chem.* **2008**, *18*, 5326–5334.
- (13) Müller, F.; Jokisch, S.; Bargel, H.; Scheibel, T. Centrifugal electrospinning enables the production of meshes of ultrathin polymer fibers. *ACS Appl. Polym. Mater.* **2020**, *2*, 4360–4367.
- (14) Thavasi, V.; Singh, G.; Ramakrishna, S. Electrospun nanofibers in energy and environmental applications. *Energy Environ. Sci.* **2008**, *1*, 205–221.
- (15) Ding, B.; Yu, J. *Electrospun Nanofibers for Energy and Environmental Applications*; Springer, 2014.
- (16) Min, X.; Sun, B.; Chen, S.; Fang, M.; Wu, X.; Liu, Y. g.; Abdelkader, A.; Huang, Z.; Liu, T.; Xi, K.; Vasant Kumar, R. A textile-based SnO<sub>2</sub> ultra-flexible electrode for lithium-ion batteries. *Energy Storage Mater.* **2019**, *16*, 597–606.

- (17) Arkoun, M.; Daigle, F.; Heuzey, M.-C.; Aji, A. Mechanism of action of electrospun chitosan-based nanofibers against meat spoilage and pathogenic bacteria. *Molecules* **2017**, *22*, 585.
- (18) Cui, H.; Bai, M.; Li, C.; Liu, R.; Lin, L. Fabrication of chitosan nanofibers containing tea tree oil liposomes against *Salmonella* spp. in chicken. *LWT* **2018**, *96*, 671–678.
- (19) Fang, Y.; Dulaney, A. R.; Gadley, J.; Maia, J.; Ellison, C. J. A comparative parameter study: Controlling fiber diameter and diameter distribution in centrifugal spinning of photocurable monomers. *Polymer* **2016**, *88*, 102–111.
- (20) Li, X.; Lu, Y.; Hou, T.; Zhou, J.; Yang, B. Centrifugally spun ultrafine starch/PEO fibres as release formulation for poorly water-soluble drugs. *Micro & Nano Lett.* **2018**, *13*, 1688–1692.
- (21) Kutzli, I.; Gibis, M.; Baier, S. K.; Weiss, J. Electrospinning of whey and soy protein mixed with maltodextrin—Influence of protein type and ratio on the production and morphology of fibers. *Food Hydrocolloids* **2019**, *93*, 206–214.
- (22) Sullivan, S. T.; Tang, C.; Kennedy, A.; Talwar, S.; Khan, S. A. Electrospinning and heat treatment of whey protein nanofibers. *Food Hydrocolloids* **2014**, *35*, 36–50.
- (23) Cheng, S. Z. D.; Chen, J.; Janimak, J. J. Crystal growth of intermediate-molecular-mass poly (ethylene oxide) fractions from the melt. *Polymer* **1990**, *31*, 1018–1024.
- (24) Tian, N.; Zhou, W.; Cui, K.; Liu, Y.; Fang, Y.; Wang, X.; Liu, L.; Li, L. Extension flow induced crystallization of poly (ethylene oxide). *Macromolecules* **2011**, *44*, 7704–7712.
- (25) Tirtaatmadja, V.; McKinley, G. H.; Cooper-White, J. J. Drop formation and breakup of low viscosity elastic fluids: Effects of molecular weight and concentration. *Phys. Fluids* **2006**, *18*, 043101.
- (26) Arnolds, O.; Buggisch, H.; Sachsenheimer, D.; Willenbacher, N. Capillary breakup extensional rheometry (CaBER) on semi-dilute and concentrated polyethyleneoxide (PEO) solutions. *Rheol. Acta* **2010**, *49*, 1207–1217.
- (27) Sharma, V.; Haward, S. J.; Serdy, J.; Keshavarz, B.; Soderlund, A.; Threlfall-Holmes, P.; McKinley, G. H. The rheology of aqueous solutions of Ethyl Hydroxy-Ethyl Cellulose (EHEC) and its hydrophobically modified analogue (hmEHEC): Extensional flow response in capillary break-up, jetting (ROJER) and in a cross-slot extensional rheometer. *Soft Matter* **2015**, *11*, 3251–3270.
- (28) Yu, J. H.; Fridrikh, S. V.; Rutledge, G. C. The role of elasticity in the formation of electrospun fibers. *Polymer* **2006**, *47*, 4789–4797.
- (29) Dinic, J.; Zhang, Y.; Jimenez, L. N.; Sharma, V. Extensional relaxation times of dilute, aqueous polymer solutions. *ACS Macro Lett.* **2015**, *4*, 804–808.
- (30) Dinic, J.; Biagioli, M.; Sharma, V. Pinch-off dynamics and extensional relaxation times of intrinsically semi-dilute polymer solutions characterized by dripping-onto-substrate rheometry. *J. Polym. Sci., Part B: Polym. Phys.* **2017**, *55*, 1692–1704.
- (31) Dinic, J.; Sharma, V. Macromolecular relaxation, strain, and extensibility determine elastocapillary thinning and extensional viscosity of polymer solutions. *Proc. Natl. Acad. Sci. U.S.A.* **2019**, *116*, 8766–8774.
- (32) Dinic, J.; Sharma, V. Flexibility, extensibility, and ratio of Kuhn length to packing length govern the pinching dynamics, coil-stretch transition, and rheology of polymer solutions. *Macromolecules* **2020**, *53*, 4821–4835.
- (33) Narváez, C. D. V. M.; Mazur, T.; Sharma, V. Dynamics and extensional rheology of polymer-surfactant association complexes. *Soft Matter* **2021**, *17*, 6116–6126.
- (34) Stojanovska, E.; Canbay, E.; Pampal, E. S.; Calisir, M. D.; Agma, O.; Polat, Y.; Simsek, R.; Gundogdu, N. A. S.; Akgul, Y.; Kilic, A. A review on non-electro nanofiber spinning techniques. *RSC Adv.* **2016**, *6*, 83783–83801.
- (35) Sarkar, K.; Gomez, C.; Zambrano, S.; Ramirez, M.; de Hoyos, E.; Vasquez, H.; Lozano, K. Electrospinning to Forc spinning. *Mater. Today* **2010**, *13*, 12–14.
- (36) Badrossamay, M. R.; McIlwee, H. A.; Goss, J. A.; Parker, K. K. Nanofiber assembly by rotary jet-spinning. *Nano Lett.* **2010**, *10*, 2257–2261.
- (37) Zhang, X.; Lu, Y. Centrifugal spinning: an alternative approach to fabricate nanofibers at high speed and low cost. *Polym. Rev.* **2014**, *54*, 677–701.
- (38) Banerji, A.; Jin, K.; Mahanthappa, M. K.; Bates, F. S.; Ellison, C. J. Porous fibers templated by melt blowing cocontinuous immiscible polymer blends. *ACS Macro Lett.* **2021**, *10*, 1196–1203.
- (39) Tan, D. H.; Zhou, C.; Ellison, C. J.; Kumar, S.; Macosko, C. W.; Bates, F. S. Meltblown fibers: Influence of viscosity and elasticity on diameter distribution. *J. Non-Newtonian Fluid Mech.* **2010**, *165*, 892–900.
- (40) Ikegame, M.; Tajima, K.; Aida, T. Template synthesis of polypyrrole nanofibers insulated within one-dimensional silicate channels: hexagonal versus lamellar for recombination of polarons into bipolarons. *Angew. Chem., Int. Ed.* **2003**, *42*, 2154–2157.
- (41) Zhao, J.; Han, W.; Chen, H.; Tu, M.; Zeng, R.; Shi, Y.; Cha, Z.; Zhou, C. Preparation, structure and crystallinity of chitosan nano-fibers by a solid–liquid phase separation technique. *Carbohydr. Polym.* **2011**, *83*, 1541–1546.
- (42) Suzuki, A.; Tanizawa, K. Poly (ethylene terephthalate) nanofibers prepared by CO<sub>2</sub> laser supersonic drawing. *Polymer* **2009**, *50*, 913–921.
- (43) Padron, S.; Fuentes, A.; Caruntu, D.; Lozano, K. Experimental study of nanofiber production through forc spinning. *J. Appl. Phys.* **2013**, *113*, 024318.
- (44) Noroozi, S.; Arne, W.; Larson, R. G.; Taghavi, S. M. A comprehensive mathematical model for nanofiber formation in centrifugal spinning methods. *J. Fluid Mech.*, **2020**, *892*, A26.
- (45) Ren, L.; Ozisik, R.; Kotha, S. P.; Underhill, P. T. Highly efficient fabrication of polymer nanofiber assembly by centrifugal jet spinning: process and characterization. *Macromolecules* **2015**, *48*, 2593–2602.
- (46) McKee, M. G.; Wilkes, G. L.; Colby, R. H.; Long, T. E. Correlations of solution rheology with electrospun fiber formation of linear and branched polyesters. *Macromolecules* **2004**, *37*, 1760–1767.
- (47) Gupta, P.; Elkins, C.; Long, T. E.; Wilkes, G. L. Electrospinning of linear homopolymers of poly (methyl methacrylate): exploring relationships between fiber formation, viscosity, molecular weight and concentration in a good solvent. *Polymer* **2005**, *46*, 4799–4810.
- (48) Shenoy, S. L.; Bates, W. D.; Frisch, H. L.; Wnek, G. E. Role of chain entanglements on fiber formation during electrospinning of polymer solutions: good solvent, non-specific polymer–polymer interaction limit. *Polymer* **2005**, *46*, 3372–3384.
- (49) Subramanian, C.; Weiss, R. A.; Shaw, M. T. Electrospinning and characterization of highly sulfonated polystyrene fibers. *Polymer* **2010**, *51*, 1983–1989.
- (50) Palangetic, L.; Reddy, N. K.; Srinivasan, S.; Cohen, R. E.; McKinley, G. H.; Clasen, C. Dispersity and spinnability: Why highly polydisperse polymer solutions are desirable for electrospinning. *Polymer* **2014**, *55*, 4920–4931.
- (51) Rošic, R.; Pelipenko, J.; Kocbek, P.; Baumgartner, S.; Bešter-Rogač, M.; Kristl, J. The role of rheology of polymer solutions in predicting nanofiber formation by electrospinning. *Eur. Polym. J.* **2012**, *48*, 1374–1384.
- (52) Lemma, S. M.; Bossard, F.; Rinaudo, M. Preparation of pure and stable chitosan nanofibers by electrospinning in the presence of poly (ethylene oxide). *Int. J. Mol. Sci.* **2016**, *17*, 1790.
- (53) Lundahl, M. J.; Berta, M.; Ago, M.; Stading, M.; Rojas, O. J. Shear and extensional rheology of aqueous suspensions of cellulose nanofibrils for biopolymer-assisted filament spinning. *Eur. Polym. J.* **2018**, *109*, 367–378.
- (54) Haward, S. J.; Sharma, V.; Butts, C. P.; McKinley, G. H.; Rahatekar, S. S. Shear and extensional rheology of cellulose/ionic liquid solutions. *Biopolymers* **2012**, *13*, 1688–1699.
- (55) Malkin, A. Y.; Semakov, A. V.; Skvortsov, I. Y.; Zatonikh, P.; Kulichikhin, V. G.; Subbotin, A. V.; Semenov, A. N. Spinnability of dilute polymer solutions. *Macromolecules* **2017**, *50*, 8231–8244.
- (56) Petrie, C. J. S. One hundred years of extensional flow. *J. Non-Newtonian Fluid Mech.* **2006**, *137*, 1–14.
- (57) Reneker, D. H.; Yarin, A. L. Electrospinning jets and polymer nanofibers. *Polymer* **2008**, *49*, 2387–2425.

- (58) Tripatanasuwan, S.; Zhong, Z.; Reneker, D. H. Effect of evaporation and solidification of the charged jet in electrospinning of poly (ethylene oxide) aqueous solution. *Polymer* **2007**, *48*, 5742–5746.
- (59) Chavez, R. O.; Lodge, T. P.; Alcoutlabi, M. Recent developments in centrifugally spun composite fibers and their performance as anode materials for lithium-ion and sodium-ion batteries. *Mater. Sci. Eng. B* **2021**, *266*, 115024.
- (60) Weitz, R. T.; Harnau, L.; Rauschenbach, S.; Burghard, M.; Kern, K. Polymer nanofibers via nozzle-free centrifugal spinning. *Nano Lett.* **2008**, *8*, 1187–1191.
- (61) Merchiers, J.; Meurs, W.; Deferme, W.; Peeters, R.; Buntinx, M.; Reddy, N. K. Influence of polymer concentration and nozzle material on centrifugal fiber spinning. *Polymers* **2020**, *12*, 575.
- (62) Merchiers, J.; Narváez, C. D. V. M.; Slykas, C.; Buntinx, M.; Deferme, W.; D'Haen, J.; Peeters, R.; Sharma, V.; Reddy, N. K. Centrifugally spun PEO fibers rival the properties of electrospun fibers. *J. Polym. Sci.* **2021**, *59*, 2754–2762.
- (63) Merchiers, J.; Narváez, C. D. V. M.; Slykas, C.; Reddy, N. K.; Sharma, V. Evaporation and rheology chart the processability map for centrifugal force spinning. *Macromolecules* **2021**, *54*, 11061–11073.
- (64) Merchiers, J.; Reddy, N. K.; Sharma, V. Extensibility-enriched spinnability and enhanced sorption and strength of centrifugally spun polystyrene fiber mats. *Macromolecules* **2022**, *55*, 942–955.
- (65) Zhmayev, Y.; Divvela, M. J.; Ruo, A.-C.; Huang, T.; Joo, Y. L. The jetting behavior of viscoelastic Boger fluids during centrifugal spinning. *Phys. Fluids* **2015**, *27*, 123101.
- (66) Mellado, P.; McIlwee, H. A.; Badrossamay, M. R.; Goss, K. P.; Mahadevan, L.; Parker, K. A simple model for nanofiber formation by rotary jet-spinning. *Appl. Phys. Lett.* **2011**, *99*, 203107.
- (67) Rashid, T. U.; Gorga, R. E.; Krause, W. E. Mechanical properties of electrospun fibers—A critical review. *Adv. Eng. Mater.* **2021**, *23*, 2100153.
- (68) Bianco, A.; Calderone, M.; Cacciotti, I. Electrospun PHBV/PEO co-solution blends: Microstructure, thermal and mechanical properties. *Mater. Sci. Eng. C* **2013**, *33*, 1067–1077.
- (69) Samad, Y. A.; Asghar, A.; Hashaikheh, R. Electrospun cellulose/PEO fiber mats as a solid polymer electrolytes for Li ion batteries. *Renewable Energy* **2013**, *56*, 90–95.
- (70) Xu, X.; Wang, H.; Jiang, L.; Wang, X.; Payne, S. A.; Zhu, J. Y.; Li, R. Comparison between cellulose nanocrystal and cellulose nanofibril reinforced poly (ethylene oxide) nanofibers and their novel shish-kebab-like crystalline structures. *Macromolecules* **2014**, *47*, 3409–3416.
- (71) Surendhiran, D.; Li, C.; Cui, H.; Lin, L. Fabrication of high stability active nanofibers encapsulated with pomegranate peel extract using chitosan/PEO for meat preservation. *Food Packag Shelf Life* **2020**, *23*, 100439.
- (72) Polaskova, M.; Peer, P.; Cermak, R.; Ponizil, P. Effect of thermal treatment on crystallinity of poly(ethylene oxide) electrospun fibers. *Polymers* **2019**, *11*, 1384.
- (73) Laramée, A. W.; Lanthier, C.; Pellerin, C. Electrospinning of highly crystalline polymers for strongly oriented fibers. *ACS Appl. Polym. Mater.* **2020**, *2*, 5025–5032.
- (74) Thompson, C. J.; Chase, G. G.; Yarin, A. L.; Reneker, D. H. Effects of parameters on nanofiber diameter determined from electrospinning model. *Polymer* **2007**, *48*, 6913–6922.
- (75) Dinic, J.; Jimenez, L. N.; Sharma, V. Pinch-off dynamics and dripping-onto-substrate (DoS) rheometry of complex fluids. *Lab Chip* **2017**, *17*, 460–473.
- (76) Dinic, J.; Sharma, V. Power laws dominate shear and extensional rheology response and capillarity-driven pinching dynamics of entangled hydroxyethyl cellulose (HEC) solutions. *Macromolecules* **2020**, *53*, 3424–3437.
- (77) Jimenez, L. N.; Dinic, J.; Parsi, N.; Sharma, V. Extensional relaxation time, pinch-off dynamics and printability of semi-dilute polyelectrolyte solutions. *Macromolecules* **2018**, *51*, 5191–5208.
- (78) Jimenez, L. N.; Narváez, C. D. V. M.; Sharma, V. Capillary breakup and extensional rheology response of food thickener cellulose gum (NaCMC) in salt-free and excess salt solutions. *Phys. Fluids* **2020**, *32*, 012113.
- (79) Narváez, C. D. V. M.; Dinic, J.; Lu, X.; Wang, C.; Rock, R.; Sun, H.; Sharma, V. Rheology and pinching dynamics of associative polysaccharide solutions. *Macromolecules* **2021**, *54*, 6372–6388.
- (80) Jimenez, L. N.; Narváez, C. D. V. M.; Xu, C.; Bacchi, S.; Sharma, V. The rheologically-complex fluid beauty of nail lacquer formulations. *Soft Matter* **2021**, *17*, 5197–5213.
- (81) Padron, S.; Patlan, R.; Gutierrez, J.; Santos, N.; Eubanks, T.; Lozano, K. Production and characterization of hybrid BEH-PPV/PEO conjugated polymer nanofibers by forcespinning. *J. Appl. Polym. Sci.* **2012**, *125*, 3610–3616.
- (82) Lu, Y.; Li, Y.; Zhang, S.; Xu, G.; Fu, K.; Lee, H.; Zhang, X. Parameter study and characterization for polyacrylonitrile nanofibers fabricated via centrifugal spinning process. *Eur. Polym. J.* **2013**, *49*, 3834–3845.
- (83) Rubinstein, M.; Colby, R. H. *Polymer Physics*; Oxford Univ. Press: New York, 2003.
- (84) Shankar, R.; Klossner, R. R.; Weaver, J. T.; Koga, T.; van Zanten, J. H.; Krause, W. E.; Colina, C. M.; Tanaka, F.; Spontak, R. J. Competitive hydrogen-bonding in polymer solutions with mixed solvents. *Soft Matter* **2009**, *5*, 304–307.
- (85) McKinley, G. H. Visco-elasto-capillary thinning and break-up of complex fluids. *Rheol. Rev.* **2005**, *1*–48.
- (86) Yarin, A. L. *Free Liquid Jets and Films: Hydrodynamics and Rheology*; Longman Scientific & Technical, 1993.
- (87) Xu, H.; Chen, H.; Li, X.; Liu, C.; Yang, B. A comparative study of jet formation in nozzle- and nozzle-less centrifugal spinning systems. *J. Polym. Sci., Part B: Polym. Phys.* **2014**, *52*, 1547–1559.
- (88) Wu, Q.; Mei, C.; Zhang, X.; Lei, T.; Zhang, Z.; Li, M. *Electrospun Poly (Ethylene Oxide) Fibers Reinforced With Poly (Vinylpyrrolidone) Polymer And Cellulose Nanocrystals*; IntechOpen, 2018.
- (89) Baji, A.; Mai, Y.-W.; Wong, S.-C.; Abtahi, M.; Chen, P. Electrospinning of polymer nanofibers: Effects on oriented morphology, structures and tensile properties. *Compos. Sci. Technol.* **2010**, *70*, 703–718.
- (90) Filip, P.; Peer, P. Characterization of poly (ethylene oxide) nanofibers—Mutual relations between mean diameter of electrospun nanofibers and solution characteristics. *Processes* **2019**, *7*, 948.
- (91) Filip, P.; Zelenkova, J.; Peer, P. Evaluation of an onset of electrospun beadless poly (ethylene oxide) nanofibers. *J. Appl. Polym. Sci.* **2021**, *138*, 50001.
- (92) Škrlec, K.; Zupančič, Š.; Mihevc, S. P.; Kocbek, P.; Kristl, J.; Berlec, A. Development of electrospun nanofibers that enable high loading and long-term viability of probiotics. *Eur. J. Pharm. Biopharm.* **2019**, *136*, 108–119.
- (93) McCullen, S. D.; Stevens, D. R.; Roberts, W. A.; Ojha, S. S.; Clarke, L. I.; Gorga, R. E. Morphological, electrical, and mechanical characterization of electrospun nanofiber mats containing multiwalled carbon nanotubes. *Macromolecules* **2007**, *40*, 997–1003.
- (94) Grothe, T.; Brikmann, J.; Ehrmann, A. In PEO as spinnable polymer and spinning-agent for non-spinnable materials. *Proceedings of Aachen–Dresden–Denkendorf International Textile Conference*; Bielefeld University of Applied Sciences, 2016.
- (95) Amiri, N.; Ajami, S.; Shahroodi, A.; Jannatabadi, N.; Amiri Darban, S.; Bazzaz, B. S. F.; Pishavar, E.; Kalalinia, F.; Movaffagh, J. Teicoplanin-loaded chitosan-PEO nanofibers for local antibiotic delivery and wound healing. *Int. J. Biol. Macromol.* **2020**, *162*, 645–656.
- (96) Kupka, V.; Dvořáková, E.; Manakhov, A.; Michlíček, M.; Petruš, J.; Vojtová, L.; Zajíčková, L. Well-blended PCL/PEO electrospun nanofibers with functional properties enhanced by plasma processing. *Polymers* **2020**, *12*, 1403.
- (97) Schabikowski, M.; Tomaszewska, J.; Kata, D.; Graule, T. Rotary jet-spinning of hematite fibers. *Textil. Res. J.* **2015**, *85*, 316–324.
- (98) Lu, Y.; Li, X.; Hou, T.; Yang, B. Centrifugally spun of alginate-riched submicron fibers from alginate/polyethylene oxide blends. *Polym. Eng. Sci.* **2018**, *58*, 1644–1651.
- (99) Alenezi, H.; Cam, M. E.; Edirisinghe, M. Experimental and theoretical investigation of the fluid behavior during polymeric fiber formation with and without pressure. *Appl. Phys. Rev.* **2019**, *6*, 041401.

(100) Li, Z.; Mei, S.; Dong, Y.; She, F.; Kong, L. High efficiency fabrication of chitosan composite nanofibers with uniform morphology via centrifugal spinning. *Polymers* **2019**, *11*, 1550.

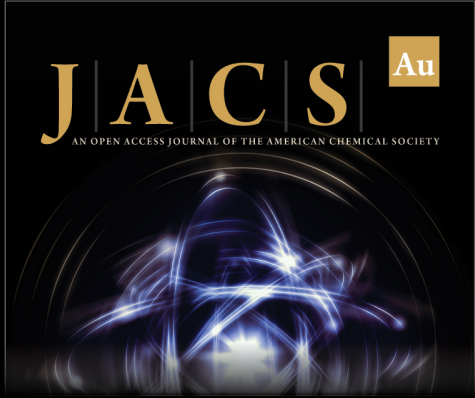
(101) Zhang, Z. M.; Duan, Y. S.; Xu, Q.; Zhang, B. A review on nanofiber fabrication with the effect of high-speed centrifugal force field. *J. Eng. Fibers Fabr.* **2019**, *14*, . DOI: [10.1177/1558925019867517](https://doi.org/10.1177/1558925019867517)

(102) Li, C.; Huang, Y.; Li, R.; Wang, Y.; Xiang, X.; Zhang, C.; Wang, D.; Zhou, Y.; Liu, X.; Xu, W. Fabrication and properties of carboxymethyl chitosan/polyethylene oxide composite nonwoven mats by centrifugal spinning. *Carbohydr. Polym.* **2021**, *251*, 117037.


(103) Matsumiya, Y.; Watanabe, H. Non-Universal features in uniaxially extensional rheology of linear polymer melts and concentrated solutions: A review. *Prog. Polym. Sci.* **2020**, *112*, 101325.


(104) Costanzo, S.; Huang, Q.; Ianniruberto, G.; Marrucci, G.; Hassager, O.; Vlassopoulos, D. Shear and extensional rheology of polystyrene melts and solutions with the same number of entanglements. *Macromolecules* **2016**, *49*, 3925–3935.


(105) Huang, Q.; Hengeller, L.; Alvarez, N. J.; Hassager, O. Bridging the gap between polymer melts and solutions in extensional rheology. *Macromolecules* **2015**, *48*, 4158–4163.



**JACS** Au  
AN OPEN ACCESS JOURNAL OF THE AMERICAN CHEMICAL SOCIETY

 Editor-in-Chief  
**Prof. Christopher W. Jones**  
Georgia Institute of Technology, USA

**Open for Submissions** 

pubs.acs.org/jacsau  ACS Publications  
Most Trusted. Most Cited. Most Read.